Rapid-Mix and Chemical Quench Studies of Ferredoxin-Reduced Stearoyl-Acyl Carrier Protein Desaturase†

Karen S. Lyle,‡ Jeffrey A. Haas,‡ and Brian G. Fox*

Department of Biochemistry, College of Agricultural and Life Sciences, University of Wisconsin, Madison, Wisconsin 53706

Received January 21, 2003; Revised Manuscript Received March 21, 2003

ABSTRACT: Stearoyl-ACP Δ9 desaturase (Δ9D) catalyzes the NADPH- and O_2-dependent insertion of a cis double bond between the C9 and C10 positions of stearoyl-ACP (18:0-ACP) to produce oleoyl-ACP (18:1-ACP). This work revealed the ability of reduced [2Fe-2S] ferredoxin (Fd) to act as a catalytically competent electron donor during the rapid conversion of 18:0-ACP into 18:1-ACP. Experiments on the order of addition for substrate and reduced Fd showed high conversion of 18:0-ACP to 18:1-ACP (∼95% per Δ9D active site in a single turnover) when 18:0-ACP was added prior to reduced Fd. Reactions of the prereduced enzyme−substrate complex with O_2 and the oxidized enzyme−substrate complex with reduced Fd were studied by rapid-mix and chemical quench methods. For reaction of the prereduced enzyme−substrate complex, an exponential burst phase ($k_{burst} = 95\ s^{-1}$) of product formation accounted for ∼90% of the turnover expected for one subunit in the dimeric protein. This rapid phase was followed by a slower phase ($k_{linear} = 4.0\ s^{-1}$) of product formation corresponding to the turnover expected from the second subunit. For reaction of the oxidized enzyme−substrate complex with excess reduced Fd, a slower, linear rate ($k_{obsd} = 3.4\ s^{-1}$) of product formation was observed over ∼1.5 turnovers per Δ9D active site potentially corresponding to a third phase of reaction. An analysis of the deuterium isotope effect on the two rapid-mix reaction sequences revealed only a modest effect on k_{burst} ($^{D}k_{burst} \sim 1.5$) and k_{linear} ($^{D}k_{linear} \sim 1.4$), indicating C−H bond cleavage does not contribute significantly to the rate-limiting steps of pre-steady-state catalysis. These results were used to assemble and evaluate a minimal kinetic model for Δ9D catalysis.

The acyl-ACP[1] desaturases insert cis double bonds into fatty acyl chains (*1*). These soluble enzymes have been found in photoauxotrophic *Euglena*, the plastid organelles of plants, and in certain microbes. Variants isolated from plants contain unique selectivities for acyl-chain length and the position of double-bond insertion (*2*−*4*). The acyl-ACP desaturases are also part of a superfamily of soluble enzymes that contain catalytically essential diiron centers (*5*). Other members of this superfamily include the bacterial hydrocarbon hydroxylases and the R2 component of ribonucleotide diphosphate reductase. In part, this superfamily is defined by the presence of two copies of the diiron binding sequence motif (D/E)-$X_{-40}EX_2H$ separated by ∼100 amino acids (*6*, *7*). Furthermore, the minimal catalytic pathway for these enzymes consists of substrate binding, electron transfer to form a diferrous center, and O_2 activation as essential prerequisites to product formation (*8*−*10*).

The recombinant castor 18:0-ACP Δ9 desaturase is the best characterized of the acyl-ACP desaturases. This enzyme has an α_2 quaternary structure. Each ∼42 kDa subunit contains a diiron center that is responsible for O_2 activation and catalysis of the desaturation reaction (*7*). Study of Δ9D by optical, Mössbauer, MCD, and resonance Raman spectroscopies revealed that the physical properties of the diiron centers can be influenced by substrate binding (*11*−*14*). Notably, MCD studies of $4e^-$ Δ9D showed that the diferrous centers contained two high-spin ferrous atoms in an equivalent square pyramidal geometry, which corresponded to the coordination observed in the 2.4 Å structure of the photoreduced enzyme (*12*, *15*). Addition of 18:0-ACP to $4e^-$ Δ9D produced changes in the MCD spectrum consistent with a change in coordination number of one of the iron atoms to four-coordinate tetrahedral and a distortion of the other iron toward trigonal bipyramidal (*12*).

Several aspects of Δ9D reactivity are unique as compared to other diiron enzymes. First, $4e^-$ Δ9D obtained from sodium dithionite reduction was only slowly reactive with O_2. In contrast, dithionite reduction of methane monooxygenase allowed single-turnover catalysis and transient kinetic studies (*16*, *17*). Second, reaction of $4e^-$ Δ9D with 18:0-ACP and 1 atm of O_2 led to the rapid formation ($k_{obsd} \sim 90\ s^{-1}$ at 24 °C) of a quasi-stable μ-1,2 peroxodiferric species

† This work was supported by National Institutes of Health Grant GM-50853 to B.G.F.

* Address correspondence to this author at 141B Biochemistry Addition, 433 Babcock Dr., University of Wisconsin, Madison, WI 53706 [telephone (608) 262-9708; fax (608) 262-3453; e-mail bgfox@biochem.wisc.edu].

‡ Trainee, NIH Institutional Molecular Biophysics Pre-Doctoral Training Grant T32 GM-08293.

[1] Abbreviations: ACP, acyl carrier protein; d_4-18:0, 9,9,10,10-d_4-18:0; 18:0-ACP, ACP with stearic acid covalently attached to ACP through a phosphopantetheine thioester bond; 18:1-ACP, ACP with oleic acid covalently attached to ACP through a phosphopantetheine thioester bond; Δ9D, 18:0-ACP Δ^9 desaturase; resting Δ9D, as-isolated form of Δ9D containing all ferric sites; $4e^-$ Δ9D, chemically reduced form of Δ9D containing all ferrous sites; Fd, *Anabaena* 7120 vegetative [2Fe-2S] ferredoxin; GC, gas chromatography; MS, mass spectrometry.

10.1021/bi030020o CCC: $25.00
Published on Web 04/19/2003

named peroxo Δ9D (*13*, *14*). Peroxo Δ9D has optical and vibrational properties that are remarkably similar to those of the peroxodiferric intermediates detected in other diiron enzymes (*18*, *19*). However, the Mössbauer spectrum of peroxo Δ9D uniquely indicated the presence of asymmetric sites within the diferric center (*13*). Decay of peroxo Δ9D was slow ($t_{1/2} \sim 26$ min) and did not result in the formation of either 18:1-ACP or H_2O_2 (*14*). These results suggested a novel oxidase reaction from Δ9D. Third, where resonance Raman studies of R2 showed that ^{18}O from $^{18}O_2$ was incorporated into the μ-oxo bridge upon single turnover and Y122$^{\bullet}$ formation (*20*), comparable studies of Δ9D showed that ^{18}O from $^{18}O_2$ was not incorporated into the μ-oxo position upon stoichiometric, rapid formation of 18:1-ACP (*11*). Moreover, the ^{18}O-atom-transfer reactions leading to the monooxygenations characteristic of MmoH and T4moH do not occur with Δ9D except during reactions with poorly reactive alternative substrate analogues (*21*, *22*). These results outline the substantial variation in metal center reactivity that has emerged within the diiron enzyme superfamily.

Another major difference in reactivity within the diiron enzyme superfamily is associated with the nature of the substrate. For ribonucleotide reductase R2, the diiron center performs a single-turnover post-translational modification of an active site tyrosine residue (*23*, *24*). Consequently, issues relating to formation of the enzyme−substrate complex, the associated order and timing of electron transfer and O_2 binding, and the stability of the enzyme−product complex are distinct from other members of this superfamily. For the diiron hydroxylases and desaturases, there are parallel requirements for the binding of a dissociable substrate, electron transfer, and O_2 binding during multiple-turnover catalysis. In the best-characterized hydroxylase reactions, the substrates are small hydrophobic molecules such as methane, toluene, and propene. In contrast, the desaturase reaction requires acyl-ACP (~10 kDa) for catalysis, which consists of a highly charged protein component (p*I* ~3.8), a phosphopantetheine prosthetic group, and a hydrophobic acyl chain of 14 carbons or longer (*25*). The substantial complexity of this substrate belies the possibility that extensive enzyme−substrate interactions may provide a dominant role in Δ9D catalysis. Indeed, the X-ray structure of Δ9D revealed a long channel extending from the surface through the interior of each subunit and passing in close proximity to the diiron center (*15*). Occupation of this channel by substrate will likely introduce substantial contacts between Δ9D, the acyl chain, and potentially other parts of ACP. In this regard, steady-state kinetic analysis of chain length selectivity revealed that V_{max}/K_M was dependent on acyl-chain length and implicated hydrophobic interactions as an energetic driving force in enzyme−substrate complex formation (*25*). More recently, fluorescence anistropy was used to evaluate binding affinities and k_{off} rates for acyl-ACPs with the oxidized enzyme (*26*). These studies indicated tight binding and a weak negative cooperativity for successive formation of the singly and doubly bound enzyme−substrate complexes. Moreover, rapid-mix anisotropy studies showed that k_{off} for 16:0-ACP was ~130-fold faster than for 18:0-ACP, implicating the stability of the enzyme−substrate complex as an important contributor to acyl-chain length selectivity.

In this work, rapid-mix and chemical quench methods were used to study the reaction of various complexes of Δ9D, 18:0-ACP, reduced Fd, and O_2. The results reveal the ability of reduced Fd to act as a catalytically competent electron donor during the rapid conversion of 18:0-ACP into 18:1-ACP. For reaction of the prereduced enzyme−substrate complex, an exponential burst phase of product formation was followed by a second phase of product formation, with the amplitude of each of these two phases corresponding to the turnover of one active site of the dimeric protein. For reaction of the oxidized enzyme−substrate complex with excess reduced Fd, a slower, linear rate of product formation was observed, potentially corresponding to a third phase of reaction. These results were used to assemble and evaluate a minimal kinetic model for the Δ9D catalysis.

MATERIALS AND METHODS

Enzymes. Δ9D and Fd were expressed, purified, and characterized as previously described (*14*, *27*, *28*). The concentration of Δ9D active sites was determined using $\epsilon_{340} = 4200\ M^{-1}\ cm^{-1}$ per diiron center and cross-correlated by determination of protein concentration and total iron *(13, 14)*. For the preparations used in this work, these quantitations indicate >95% occupation of diiron active sites in the dimeric protein. Furthermore, the specific activity of the Δ9D preparations used in this work matched that observed for the maximally active enzyme *(22, 25)*. Recombinant *Escherichia coli* ACP was expressed, purified, phosphopantetheinylated, and acylated as previously described (*29*, *30*). Acyl chains were reductively cleaved, extracted, derivatized, and analyzed by GC-MS as previously described (*25*).

Synthesis of 9,9,10,10-d_4-Stearic Acid. The deuterated fatty acid was prepared from stearolic acid by homogeneous hydrogenation using Wilkinson's catalyst (99.9%, Aldrich, Milwaukee, WI) and D_2 gas (99.6% D_2, 0.4% HD, Cambridge Isotope Laboratories, Andover, MA) (*31*) and purified by cation exhange (AG 50W-X4 resin, Bio-Rad, Hercules, CA). An average deuterium content of ~97% was estimated from MS scans within the peak corresponding to the *N*-methyl-*N*-(trimethylsilyl)trifluoroacetamide derivative. The d_4-18:0 was covalently attached to *E. coli* holo-ACP as previously described (*29*), and the reaction workup was identical to that used for the unlabeled compound. The deuterated compounds were analyzed by integrating the peak areas containing the substrate (*m*/*z* 331 amu for the M − 15 peak) and the desaturated product (*m*/*z* 327 amu for the M − 15 peak).

Fd Preparations. Reduced Fd was made by placing a solution of oxidized Fd in a septum-sealed cuvette modified to contain a two-way stopcock. This solution was made anaerobic by repeated cycling between vacuum and refill with O_2-free Ar. The oxidized Fd was reduced by titration with a solution of ~0.1 M $Na_2S_2O_4$ prepared in anaerobic 1 M sodium phosphate buffer, pH 7.0, until the ratio A_{398}/A_{422} was ≥1.2. The oxidation rate of reduced Fd was determined at room temperature by stopped-flow optical spectrometry using an RSM 1000F spectrophotometer (OLIS, Bogart, GA) with a 400 lines/mm grating centered at 500 nm. The reaction was initiated by rapidly mixing equal volumes of aerobic 50 mM Hepes, pH 7.0, containing 35 mM NaCl and 100 μM reduced Fd. Single-value decomposition analysis was used to extract apparent first-order rate constants for the conversion from reduced Fd to oxidized Fd.

Hand-Mixed Experiments. Product formation was assessed by hand-mixing a 500 μL solution of 50 μM Δ9D active sites (either with or without 18:0-ACP and/or O_2) with an equal volume of reduced Fd. The buffer was 50 mM Hepes, pH 7.0, containing 35 mM NaCl, and the reactions were performed at room temperature. Immediately after mixing, the stoichiometry of 18:0-ACP to 9D active sites was 1:1 and that of reduced Fd to Δ9D 4:1. The solution was gently mixed by hand motion, and a 200 μL aliquot of the solution was removed and mixed with 150 μL of tetrahydrofuran to quench the enzyme reaction.

Rapid-Mix Chemical Quench Experiments. These experiments were performed at room temperature using a System 1000 rapid-mix chemical quench apparatus (Update Instrument, Inc., Madison, WI) equipped with a model 715 ram controller and model 1019 syringe ram. The buffer was 50 mM HEPES, pH 7.8, containing 35 mM NaCl.

For single-turnover experiments in which reduced Fd was added by rapid-mix, syringe 1 was filled with 1 mL of aerobic buffer containing 150 μM 18:0-ACP and 50 μM Δ9D active sites, and syringe 2 was filled with 1 mL of buffer containing either 50, 100, or 200 μM reduced Fd. For multiple-turnover experiments, syringe 1 contained 1 mL of aerobic buffer containing 500 μM 18:0-ACP and 50 μM Δ9D active sites, and syringe 2 was filled with 1 mL of buffer containing 400 μM reduced Fd. For experiments in which reduced Fd, Δ9D, and 18:0-ACP were preincubated prior to rapid-mix with aerobic buffer, the reduced Fd was prepared as described above and transferred to an anaerobic glovebox chamber (Coy Laboratory Products Inc., Grass City, MI), where it was mixed with a solution containing anaerobic Δ9D and 18:0-ACP. The final concentration of the reaction components in syringe 1 was 500 μM 18:0-ACP and either 50 μM or 100 μM Δ9D active sites. The reduced Fd concentration was 400 μM in order to provide an 8- or 4-fold excess of reducing equivalents relative to Δ9D active sites. Syringe 1 was filled with 1 mL of this mixture in the anaerobic glovebox chamber, whereas syringe 2 was filled with 1.0 mL of aerobic buffer outside the anaerobic chamber. Prior to removal from the anaerobic chamber, any syringes containing reduced Fd were capped to slow the entry of O_2.

The syringes were transferred to the rapid-mix device, and the total preincubation period before the rapid mixing experiment was ~10 min. Aging tubes and programmed delays giving 11−1000 ms reaction times were used for data collection. The rapid-mix samples exiting the aging tubes were quenched into 200 μL of tetrahydrofuran. After completion of the experiment, the remaining volume of syringe 1 was removed and quenched in the anaerobic chamber to provide a background control, and <1% conversion to 18:1-ACP was observed. The quenched samples were diluted with distilled and deionized water to 800 μL. The acyl chains were reductively cleaved from ACP, extracted, and analyzed by tandem GC-MS (*25*).

Data Analyses. For Δ9D reactions exhibiting burst kinetics, the apparent rate constants were calculated from the product formation data with the NonlinearRegress routine (Mathematica v. 4.0.1.0, Wolfram Research, Champaign, IL) using the Levenberg−Marquardt method, infinite maximum iterations, and default options for other adjustable calculation parameters. Equations suitable for the evaluation of burst kinetic data have been previously derived (*32*), and eq 1 was used as the target function

$$p(t) = \left(\frac{a_1}{(a_1 + a_3)}\right)^2 [\mathrm{enz}](1 - \exp[-(a_1 + a_3)](\mathrm{d}t)) + \left(\frac{a_1 a_3 [\mathrm{enz}](\mathrm{d}t)}{(a_1 + a_3)}\right) \quad (1)$$

where $p(t)$ is the calculated time-dependent product accumulation, a_1 and a_3 are the rate constants associated with the fast and slow phases of the burst reaction, respectively, and [*enz*] is the enzyme concentration. In the fitting procedure, [*enz*] was an experimental constant value, whereas a_1 and a_3 were fitting parameters. Equation 2 (*32*) was used to calculate the burst amplitude as a percentage of enzyme active site concentration:

$$A_{\mathrm{burst}} = 100[a_1/(a_1 + a_3)]^2 \quad (2)$$

The abilities of different kinetic models to account for the experimental results were evaluated by numerical simulation using the Mathematica NDSolve routine. For each kinetic scheme investigated, the definitions required for the simulation included initial boundary conditions for all enzyme, substrate, and product species as defined by the kinetic scheme, a mass balance expression accounting for all enzyme species present, and differential equations describing the time-dependent interconversions of these species (*33*). Statistical factors accounting for multiple pathways leading to the same enzyme species were included in the differential equations. Experimentally determined rates were assigned as constants to the appropriate steps of the kinetic models, whereas rate constants for substrate binding and product release steps were assigned initial values based on estimates from previous experiments (*26*). The reaction steps associated with electron transfer and chemical catalysis were assigned to be irreversible, whereas substrate binding and product release were considered to be reversible and dependent on the changing concentrations of substrate and product generated during the simulation. The results of the numerical simulation were evaluated by comparison with the experimental results using visual inspection, because model-dependent differences in the simulation results were clearly recognized as indicated under both Results and Discussion.

RESULTS

Order of Substrate and Fd Addition. Previous studies of Δ9D have shown that reaction of $4e^-$ Δ9D produced by sodium dithionite did not result in the formation of 18:1-ACP during a single turnover but instead gave rise to peroxo Δ9D (*14*). Here, reduced Fd is shown by rapid-mix, chemical quench studies to act as a catalytically competent electron donor for single-turnover reactions of Δ9D leading to 18:1-ACP formation.

Because a complete steady-state kinetic analysis of Δ9D indicating the order of binding of 18:0-ACP, reduced Fd, and O_2 has not yet been completed,[2] the most favorable order of addition was investigated using hand-mixed experiments as a prerequisite to the more demanding rapid-mix experiments. Figure 1A shows a schematic of the mixing sequences

[2] K. S. Lyle and B. G. Fox, unpublished results.

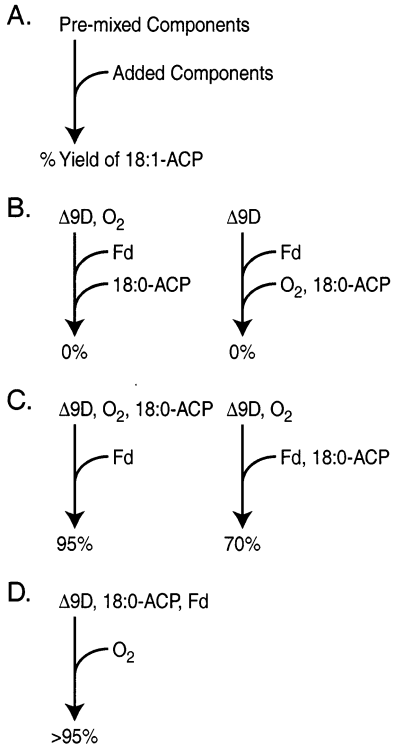

FIGURE 1: Investigation of mixing order and 18:1-ACP yield using Δ9D, 18:0-ACP, reduced Fd, and O_2. 18:1-ACP yields are reported as the percentage of Δ9D active sites: (A) schematic representation of premixed components, added component(s), and 18:1-ACP yield. (B) Reactions in which aerobic Δ9D preparations were premixed with reduced Fd followed by 18:0-ACP. (C) Reactions in which aerobic Δ9D and 18:0-ACP were premixed either prior to or concomitant with addition of reduced Fd. (D) Reaction in which anaerobic Δ9D, reduced Fd, and 18:0-ACP were premixed with aerobic buffer. After mixing, the concentrations were 25 μM Δ9D active sites, 25 μM 18:0-ACP, and 100 μM reduced Fd. In reactions with aerobic Δ9D, the O_2 concentration upon mixing was ~125 μM, whereas O_2 (1 atm) was added to reactions initiated with anaerobic Δ9D.

used for these reactions and identifies the premixed components, the added component(s), and the resultant yield of 18:1-ACP. In the best circumstances, these reactions required ~5 s to mix the solution and remove an aliquot for chemical quench and product analysis.

Figure 1B shows that reaction of excess reduced Fd with either aerobic or anaerobic Δ9D samples prior to the addition of 18:0-ACP gave no 18:1-ACP formation. In contrast, Figure 1C shows that 18:1-ACP was produced when 18:0-ACP was mixed with Δ9D either prior to or concomitant with the addition of reduced Fd. In the experiments of Figure 1C, up to ~95% yield of 18:1-ACP per active site was obtained. Figure 1D shows another mixing sequence in which a pre-equilibrated solution of Δ9D, 18:0-ACP, and excess reduced Fd was mixed with aerobic buffer. This reaction sequence also gave a high yield of 18:1-ACP product. Due to the comparable yields obtained, these latter two reaction sequences were further investigated using rapid-mix methods.

Characterization of Fd Reactions. Figure 2 shows a kinetic scheme relevant to the use of reduced Fd as the reductant for Δ9D in aerobic solutions. The desaturase reaction pathway (k'_{cat}) requires the consumption of 2 mol of reduced Fd for each mol of 18:1-ACP produced, whereas the autoxidation pathway (k_{autox}) can proceed by the independent

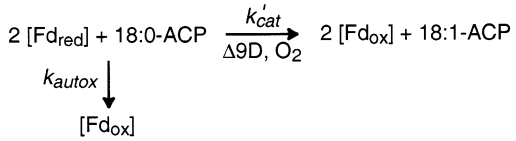

FIGURE 2: Kinetic scheme showing desaturase (k'_{cat}) and autoxidation (k_{autox}) reactions of reduced Fd in the presence of aerobic buffer and Δ9D reaction components.

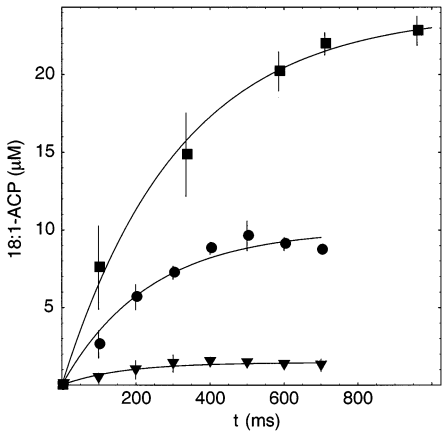

FIGURE 3: Pre-steady-state formation of 18:1-ACP during reaction of Δ9D in the presence of varied concentrations of reduced Fd. Syringe 1 of the rapid mixer contained 150 μM 18:0-ACP and 50 μM Δ9D active sites as described under Materials and Methods. Syringe 2 contained 50 μM reduced Fd (▼, $k'_{cat} = 6.1 \pm 0.5$ s^{-1}), 100 μM reduced Fd (●, $k'_{cat} = 4.2 \pm 1.5$ s^{-1}), or 200 μM reduced Fd (■, $k'_{cat} = 3.2 \pm 1.4$ s^{-1}). The solid lines are nonlinear least-squares fit to a single exponential, $a(t) = a_0\ (1 - \exp[-k'_{cat}\ t])$, with k'_{cat} indicated above. Each data point represents the average of three or more experiments, and the error bars represent 2σ deviation. Error bars for some data points were within the dimensions of the plotting symbol and are not visible.

consumption of 1 mol of reduced Fd. The partition of reduced Fd between catalysis and autoxidation depends on the relative rates for these two different reaction pathways. In aerobic buffers, the autoxidation product was presumed to be O_2^- upon the basis of the results of other studies (*34*). For the reaction of 50 μM reduced Fd alone, an apparent $k_{autox} \approx 4$ s^{-1} was determined. However, when both oxidized Δ9D and 18:0-ACP were present, the apparent rate for the formation of 18:1-ACP (see below) was similar to k_{autox}. The presence of the enzyme−substrate complex must substantially change the partition between the two pathways of Figure 2, leading to desaturation catalysis.

Fd Concentration Dependence in Transient State 18:1-ACP Formation. These experiments correspond to the order of addition shown in Figure 1C (left), the rapid-mix of the preformed aerobic complex of Δ9D and 18:0-ACP with reduced Fd. Figure 3 shows how different concentrations of reduced Fd changed the rate and yield of 18:1-ACP. In the rapid-mix experiment, the rate of 18:1-ACP formation was overall similar within experimental error at the three concentrations examined. Figure 3 also shows that the yield of 18:1-ACP increased as the concentration of reduced Fd was increased. To achieve ~1 turnover per Δ9D active site, 4 equiv of reduced Fd was required per Δ9D active site. Because the reaction stoichiometry requires 2 eq of reduced ferredoxin per 1 equiv of 18:1-ACP formed, this dependence of 18:1-ACP yield on the concentration of Fd suggested a maximal coupling between reduced Fd utilized and 18:1-

Table 1: Kinetic Parameters Obtained for Pre-Steady-State Reactions of Δ9D[a]

		burst phase			linear phase	
premix components[b]	additions[c]	k_{burst}	A_{burst}[d] (%)	$^{D}k_{burst}$	k_{linear}	$^{D}k_{linear}$
50 μM Δ9D, 18:0, Fd	O_2	95 (25)	92 (3)	1.5 (0.5)	4.0 (0.6)	1.4 (0.4)
+ d_4-18:0	O_2	63 (20)	91 (4)		2.9 (0.4)	
25 μM Δ9D, 18:0, Fd	O_2	65 (20)	85 (2)	nd[e]	5.4 (0.3)	nd
Δ9D, 18:0, O_2	Fd	−[f]	−	−	3.4 (0.1)	1.4 (0.4)

[a] Rates (k_{burst}) and burst amplitudes (A_{burst}) were obtained from nonlinear least-squares fitting with eq 1 as described under Materials and Methods. [b] Reaction components that were premixed in syringe 1. [c] Reaction component added from syringe 2 upon rapid mixing. [d] Calculated from eq 2. [e] Not determined. [f] Burst kinetics were not observed with this mixing sequence.

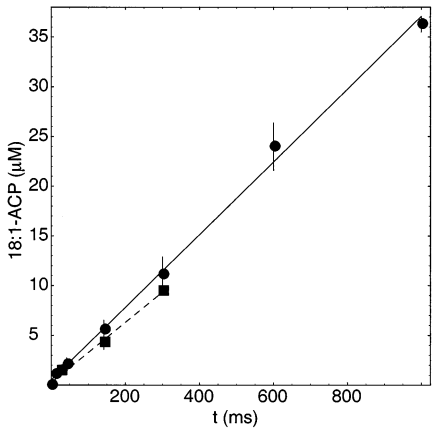

FIGURE 4: Pre-steady-state formation of 18:1-ACP during rapid-mix reaction of an aerobic complex of Δ9D and 18:0-ACP with reduced Fd. Syringe 1 of the rapid mixer contained 400 μM reduced Fd. Syringe 2 contained 50 μM Δ9D active sites and either 500 μM 18:0-ACP (●) or 500 μM d_4-18:0-ACP (■). The solid and dashed lines are linear least-squares fits. Data point averaging and error representation are as indicated in the caption to Figure 3.

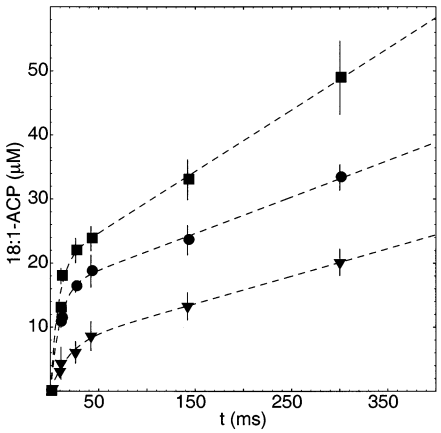

FIGURE 5: Pre-steady-state formation of 18:1-ACP during rapid-mix reactions of a prereduced, anaerobic complex of Δ9D and 18:0-ACP with aerobic buffer. Syringe 1 contained 100 μM of Δ9D active sites and 500 μM 18:0-ACP (■), 100 μM of Δ9D active sites and 500 μM d_4-18:0-ACP (●), or 50 μM of Δ9D active sites and 500 μM 18:0-ACP (▼). All reactions contained 400 μM reduced Fd. Syringe 2 contained air-saturated buffer. The dashed lines are nonlinear least-squares fits to eq 1 performed as described under Materials and Methods. Data averaging and error representation are as indicated in the caption to Figure 3.

ACP formed of ~50% in the conditions of the rapid-mix reactions. As no additional product was observed after ~1 s, autoxidation reactions (k_{autox}) must have begun to compete with one or more rate-limiting steps in the longer time regime required for multiple catalytic turnovers.

Reaction of Premixed Δ9D, 18:0-ACP, and O_2 with Reduced Fd. Figure 4 shows the initial 1 s of the reaction of a preformed aerobic complex of Δ9D and 18:0-ACP with reduced Fd (solid circles; solid line). These experiments also correspond to the order of addition shown in Figure 1C (left). Relative to the experiments of Figure 3, the concentration of 18:0-ACP was increased by 3-fold to ensure substrate saturation even after partial turnover (*26*). This experimental condition eliminates the requirement for substrate binding during the first turnover of each active site of the Δ9D dimer. Therefore, these reactions may potentially encompass the contributions of electron transfer, O_2 binding, chemical reactions, or product release steps of catalysis. In the time scale of the rapid-mix experiments, ~1.5 turnovers were obtained with an apparent 18:1-ACP formation rate of $k_{obsd} \approx 3.4\ s^{-1}$.[3] This observed rate was faster than the turnover number for 18:0-ACP previously determined by steady-state catalysis, $V_{max} = k_{cat} = 0.5-0.7\ s^{-1}$ (*25*, *29*, *35*). Identical reactions performed using d_4-18:0-ACP (solid squares; dashed line) gave an apparent d_2-18:1-ACP formation rate of $k_{obsd} \approx 2.4\ s^{-1}$, indicating a modest primary kinetic isotope effect of 1.4 for 18:1-ACP formation under these experimental conditions. The kinetic parameters obtained from these experiments are summarized in Table 1.

Reaction of Premixed Δ9D, 18:0-ACP, and Reduced Fd with O_2. These experiments correspond to the order of addition shown in Figure 1D, a rapid-mix of the preformed anaerobic complex of Δ9D, 18:0-ACP, and reduced Fd with aerobic buffer. Due to the time required for sample preparation, Δ9D was most likely converted to a fully reduced state for these experiments,[4] whereas the 18:0-ACP concentration assured substrate saturation. Consequently, this experimental condition eliminates the requirements for both substrate binding and electron transfer during the first turnover of each active site of the Δ9D dimer.

Figure 5 shows that a burst of 18:1-ACP formation occurred within the first 50 ms of rapid mixing and was followed by a further, approximately linear increase in 18:1-ACP formation during the remainder of the 300 ms reaction time. For the reaction of 50 μM Δ9D active sites (solid squares), nonlinear least-squares fitting of the experimental data using eq 1 gave $a_1 = k_{burst} = 95 \pm 25\ s^{-1}$ and $a_3 =$

[3] Numerical analysis suggests that product formation may not be "linear" in this region, but a linear least-squares analysis is presented at this point as a provisional result. Further elaboration is provided under both Results and Discussion.

[4] Mössbauer studies indicate that incubation with reduced Fd on the time scale required to prepare the samples in the anaerobic chamber gave complete reduction of the Δ9D diiron centers in the absence of 18:0-ACP. K. S. Lyle, J. A. Haas, V. Vrajmasu, E. Münck, and B. G. Fox, unpublished results.

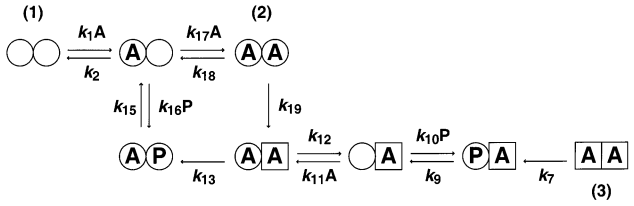

FIGURE 6: Kinetic scheme for desaturation catalyzed by Δ9D: (○) Δ9D subunit containing a diferric center; (□) Δ9D subunit containing a diferrous center. Occupation of individual subunits by substrate (A) and product (P) is as indicated. Rate constants k_7 and k_{13} indicate irreversible chemical reactions, k_9/k_{10}P and k_{15}/k_{16}P indicate reversible product binding equilibria, k_1A/k_2, k_{11}A/k_{10}, and k_{17}A/k_{18} indicate reversible substrate binding equilibria, and k_{19} indicates irreversible electron transfer.

$k_{linear} = 4.0 \pm 0.6$ s^{-1}. An analysis of the burst amplitude using eq 2 revealed that 18:1-ACP formation accounted for 90% of expected turnover for one subunit, whereas a similar amount of 18:1-ACP was formed during the linear phase within the next 250 ms of the reaction. Other experiments showed that the burst amplitude was proportional to the Δ9D concentration (Figure 5, solid triangles). Fitting results for the experiments of Figure 5 are presented in Table 1. When the burst reaction was performed using d_4-18:0-ACP (Figure 5, solid circles), $k_{burst} = 63 \pm 20$ s^{-1} and $k_{linear} = 2.9 \pm 0.4$ s^{-1} were determined, whereas the burst amplitude was again ~90%. An analysis of the deuterium isotope effect on the burst phase (*36*) gave $^{D}k_{burst} = (k_H/k_D)_{burst}$ $(A_H/A_D) = 1.5 \pm 0.5$, whereas for the linear phase, $^{D}k_{linear} = (k_H/k_D)_{linear} = 1.4 \pm 0.4$.

Kinetic Model for Δ9D Catalysis. Figure 6 shows a kinetic model for catalysis by Δ9D. In this representation, the circle symbols represent a Δ9D subunit containing a diferric center and the square symbols represent a Δ9D subunit containing a diferrous center. This model includes irreversible electron transfer (k_{19}) and irreversible chemical reaction (k_7 and k_{13}) steps. Because reduced Fd is in excess, k_{19} has been provisionally assigned to be irreversible. Moreover, the chemical reaction steps likely include O_2 activation, C−H bond cleavage, and double-bond insertion, an energetically demanding sequence that is overall irreversible. Equilibrium binding interactions between the oxidized, substrate-free enzyme (Figure 6, **1**) and the oxidized, substrate-saturated enzyme (Figure 6, **2**) have been previously investigated, corresponding to $K_{eq1} = k_1$A/k_2 and $K_{eq2} = k_{17}$A/k_{18} of Figure 6 [(*26*), with the original definition of $K_{eq2} = k_3$A/k_4]. The equilibrium constants determined previously indicate saturation of Δ9D with 18:0-ACP in the concentration regime used for these experiments. The oxidized, substrate-saturated enzyme (Figure 6, **2**) can undergo electron transfer (k_{19}) to initiate single-turnover reactions. Moreover, to account for the burst kinetic results, the fully reduced dimer saturated with substrate may also initiate the reaction (Figure 6, **3**). To account for multiple-turnover reactions, the model includes a loop with reversible equilibrium binding interactions for product release (k_{15}/k_{16}P) and substrate binding (k_{17}A/k_{18}), irreversible electron transfer (k_{19}), and a chemical reaction (k_{13}).

Equation 3 shows the expression for V_{max} within the steady-state loop of Figure 6 as given by effective rate constant analysis (*37*)

$$V_{max} = \frac{1}{\frac{1}{k_{13}} + \frac{k_{16}\text{P}(k_{18}+k_{19}) + k_{17}k_{19}\text{A}}{k_{15}k_{17}k_{19}\text{A}} + \frac{(k_{18}+k_{19})}{k_{17}k_{19}\text{A}} + \frac{1}{k_{19}}} \quad (3)$$

where the k_i values are rate constants defined in the kinetic model, A is substrate, and P is product. If initial velocity conditions (i.e., substrate saturation and no product present) are assumed, product release and substrate binding steps are effectively irreversible, allowing facile estimation of V_{max} through simplification of eq 3.

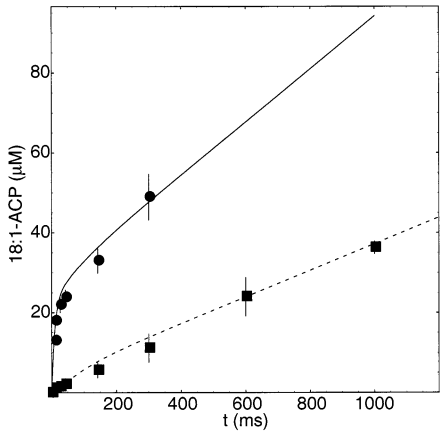

FIGURE 7: Numerical simulations of Δ9D turnover based on the kinetic model of Figure 6. The experimental data are from Figure 4 (■) and Figure 5 (●). The solid and dashed lines are simulation results obtained using the following rate constants: k_7, $k_{13} = 95$ s^{-1}; k_9, $k_{15} = 4.0$ s^{-1}; k_{10}P = k_{16}P < 0.05 M^{-1} s^{-1}; k_{11}A = k_{17}A > 1000 M^{-1} s^{-1}; $k_{12} = k_{18} = 1$ s^{-1}; $k_{19} = 3.4$ s^{-1}.

Figure 7 shows the results of numerical simulations based on the kinetic model of Figure 6. For the simulations, one goal was to determine whether a single, consistent set of experimental rate constants could reproduce the results obtained from the rapid mix of oxidized Δ9D with reduced Fd (Figure 4) and from the burst reaction of prereduced Δ9D with O_2 (Figure 5). A further goal was to test whether the simulation would predict the experimentally determined steady-state turnover after extrapolation to longer time periods. Visual inspection shows a close match between the calculated product formation (solid and dashed lines) and the experimental data obtained in the 10−1000 ms time regime, including both the single-turnover reactions proceeding from the rapid mix of oxidized Δ9D with reduced Fd (Figure 4) and the burst reaction of prereduced Δ9D with O_2 (Figure 5).

Depending on the reaction (Figure 4 or 5), the enzyme was initially assigned to be present as either **2** or **3** as defined by Figure 6. The chemical steps k_7 and k_{13} were assigned the value of $k_{burst} = 95$ s^{-1}, the product release steps, k_9 and k_{15}, were assigned the value of $k_{linear} = 4.0$ s^{-1}, and the electron-transfer step $k_{19} = 3.4$ s^{-1} was assigned from the k_{obsd} value measured in reaction of oxidized Δ9D with reduced Fd (Figure 4). Although the simulation was sensitive to the magnitude of the product release rate, it was insensitive to bimolecular steps involving product binding (product inhibition) in the initial velocity time regime, as k_{10}P = k_{16}P ≈ 0. The simulation was also insensitive to changes in the

Table 2: Comparison of Rate Constants for Reactions Catalyzed by Diiron Enzymes

enzyme and substrates	reaction	products	rate[a] (s^{-1})	k_H/k_D[b]	ref
Δ9D					
4e-Δ9D	autoxidation[c]		<0.00003		*14*
4e-Δ9D, 18:0-ACP	oxidase[d]	2 H_2O	0.00045		*14*
Δ9D, reduced Fd, Fdr 18:0-ACP, NADPH	steady-state desaturation	18:1-ACP	0.5−0.7		*25*, *29*, *35*
(Δ9D, 18:0-ACP, O_2) mixed with reduced Fd	single-turnover desaturation	18:1-ACP	3−4	1.4	this work
(Δ9D, 18:0-ACP, reduced Fd) mixed with O_2	single-turnover burst	18:1-ACP	70−120	1.5	this work
(Δ9D, 18:0-ACP, reduced Fd) mixed with O_2	single-turnover 2nd reaction	18:1-ACP	4−5	1.4	this work
stearoyl-CoA desaturase (SCD)[e]					
SCD, 18:0-CoA, cytochrome b_5	steady-state desaturation	18:1-CoA		7	*49*
RNR R2[f]					
Y122F	autoxidation		0.07		*62*
mouse apo + Fe^{2+}	oxidase	Y122•	0.29		*63*
mouse Y122		Y122•	5		*63*
Escherichia coli Y122		Y122•	0.7−1		*62*, *64*
MmoH[f]					
MmoH	autoxidation		0.02		*65*
MmoH + MmoB	autoxidation		0.3		*65*
MmoH, MmoB, MmoR + CH_4	steady-state hydroxylation	CH_3OH	0.6	1.6	*55*, *56*
MmoH + MmoB + CH_4	single-turnover hydroxylation	CH_3OH	8[g]	80	*55*

[a] O_2 required for all reactions. Turnover number per diiron center. [b] Kinetic isotope effect measured for indicated reactions. [c] Autoxidation leading to undefined products from O_2. [d] Oxidase reaction yielding 2 mol of H_2O without other substrate oxidation. [e] Assigned to an integral membrane superfamily of diiron enzymes (*66*). [f] Rates were determined at 4 or 5 °C. [g] Pseudo-first-order rate constant with 0.5 mM methane. The second-order rate constant for this reaction is 16000 s^{-1} M^{-1} (*55*).

substrate binding and dissociation rates in the initial velocity time regime due to the presence of saturating substrate, and the bimolecular rate constants for substrate binding $k_1A = k_{11}A = k_{17}A > 1000$ M^{-1} s^{-1} gave simulation results compatible with the experimental data. Correspondingly, fluorescence anisotropy studies suggested that k_1A may be of this order of magnitude or larger (*26*). For the numerical simulation, the substrate dissociation rates $k_2 = k_{12} = k_{18} = 1 \pm 0.1$ s^{-1} were assigned from previous anisotropy studies.

The use of eq 3 provides an important constraint on the validity of the rate constant assigments. Permutations of these values among the different rate constants within the catalytic loop resulted in an inability of the numerical simulation to mimic the transient kinetic data even as the effective rate constant for steady-state catalysis could be reproduced. For example, interchange of the values for k_{13} (chemical step) and k_{15} (product release) did not reproduce the second phase of the burst experiment, whereas the effective rate constant value was unchanged.

It is important to note that the simulation duplicated the experimental results from two distinct types of reactions without a change in adjustable parameters other than the appropriate assignment of initial concentrations of enzyme species. Moreover, a minimal set of unique rate constant values was required for the simulation, as $k_7 = k_{13}$, $k_9 = k_{15}$, and $k_1A = k_{11}A = k_{17}A$.

The burst reaction requires one pass through the kinetic steps from k_7 through k_{13}, whereas the catalytic loop contains k_{19}. The two phases of the experimental burst were well-reproduced by the simulation, and the presence of k_{13} in both the burst and catalytic loop of the model serves to constrain the acceptable variation in rate constant values. Upon evaluation of eq 3, given from an effective rate constants analysis, $V_{max} = k_{cat} = 1.3$ s^{-1} per active site was determined from the rate constants used for the simulation. Extension of the numerical simulation into the 100−120 s time domain showed that the total rate of product formation was dependent on enzyme concentration, and also corresponded to $k_{cat} \approx 1$ s^{-1} per active site for both experiments. For comparison, $k_{cat} \approx 0.5-0.7$ s^{-1} has been measured in steady-state catalysis (*25*, *29*, *35*). The close match of the calculated and experimental values provides substantial support for the validity of the proposed kinetic model.

DISCUSSION

This work shows results from the rapid-mix of Δ9D and 18:0-ACP leading to high-yield formation of 18:1-ACP. The accumulating experimental evidence indicates that several aspects of Δ9D catalysis are dominated by interactions with 18:0-ACP (*25*). Moreover, the importance of reduced Fd as a catalytically competent electron donor for the desaturase reaction has now been documented. The information presented here substantially extends our understanding of the unique features of Δ9D reactivity relative to other well-characterized diiron enzymes.

Role of Fd in Δ9D Reaction. Physiological electron transfer to diiron enzymes requires the formation of a complex with either a multidomain, flavin- and [2Fe-2S]-containing ferredoxin:NADH oxidoreductase, or a separate [2Fe-2S]-containing ferredoxin (*8*, *38*, *39*). However, chemical reduction by sodium dithionite has facilitated in vitro single-turnover hydroxylations (*40*, *41*) and later transient kinetic studies (*16*, *42*) catalyzed by methane monooxygenase (Table 2). Moreover, although reactions of the ribonucleotide reductase R2 component are most often initiated by reconstitution of apo-enzyme with ferrous ion (*43*, *44*), sodium dithionite-mediated reduction of the preassembled diferric center has also been studied (Table 2) (*45*). For these two diiron enzymes, the reactions of the dithionite-reduced preparations led to catalysis with rates entirely consistent with the biological processes. In contrast, reduction of the Δ9D−substrate complex with sodium dithionite led to a quasi-stable peroxodiiron(III) intermediate that decayed by an oxidase reaction and that did not yield the 18:1-ACP product (*14*).

The present studies show that reduced Fd acts as a kinetically competent reductant, leading to the formation of

18:1-ACP. Because reduced Fd was obtained by chemical reduction with sodium dithionite, the difference between catalysis and peroxo Δ9D formation apparently corresponds to the presence of reduced Fd in the enzyme reaction. Thus, an unanticipated role for reduced Fd in the Δ9D reaction is suggested.

Rapid-Mix Reaction of Δ9D. Reaction of the preformed complex of Δ9D, 18:0-ACP, and reduced Fd with O_2 buffer led to the rapid, high-yield formation of 18:1-ACP. Because lower yields of 18:1-ACP were obtained from mixing the components in other arrangements, the results anticipate an optimal kinetic order for the enzyme reaction.[2] The combined results of Figures 4 and 5 further suggest that the Δ9D reaction may consist of at least two, but possibly three, distinct kinetic phases. In the rapid-mix reactions of the prereduced enzyme−substrate complex (Figure 5), a burst phase ($k_{burst} \approx 95$ s^{-1}) was observed with an amplitude suggesting the turnover of one subunit of the dimeric enzyme ($A_{burst} \approx 90\%$). This reaction was followed by a second, linear phase of product accumulation ($k_{linear} \approx 4$ s^{-1}), ultimately leading to a total product yield comparable to that expected for the turnover of both subunits of the dimeric enzyme. For comparison, rapid-mix reactions of the oxidized enzyme−substrate complex (Figure 4) with reduced Fd gave an apparently linear product accumulation over ~1.5 turnovers per enzyme subunit with $k_{obsd} \approx 3.4$ s^{-1}, possibly corresponding to an electron-transfer phase or other rate-limiting steps in a multiple-turnover reaction cycle.

Kinetic Model for Desaturase Reaction. An equilibrium binding model for conversion of the substrate-free, oxidized Δ9D dimer (Figure 6, **1**) to the singly and doubly bound oxidized dimer (Figure 6, **2**) has been previously investigated (*26*). For catalysis, additional required steps include electron transfer, O_2 binding and activation, C−H bond cleavage, and, during multiple turnovers, product release and substrate binding. Previous studies showed that acyl-ACP amplifies the O_2 reactivity of Δ9D by ~10^4-fold, implying that 18:0-ACP binding may precede O_2 binding in the catalytic mechanism (*14*). Furthermore, hand-mixing experiments described in this work indicate that 18:0-ACP binding may occur prior to electron transfer from reduced Fd. On the basis of these considerations, the minimal kinetic model for Δ9D reactivity shown in Figure 6 was developed and investigated.

Numerical simulations of the reaction results based on the kinetic model of Figure 6 support the assignment of the burst phase to an irreversible chemical step of the desaturation reaction (k_7 and k_{13}), whereas the linear phase was assigned to a partially rate-limiting product release step (k_9 and k_{15}) situated between successive rapid equilibrium ($k_{11}A/k_{12}$) and irreversible chemical (k_{13}) steps. Simulations derived from this model reproduced experimental variations including the protein concentration and the redox state of Δ9D at the start of the reaction with no adjustable parameters required other than a proper assignment of the initial enzyme species concentrations and the desired time regime for reaction. During multiple turnovers proceeding through the catalytic loop of Figure 6, the V_{max} expression given by eq 3 includes significant contributions from electron transfer and product release and a lesser contribution from the chemical reaction. Thus, all of these steps contribute to the rate limitation of steady-state catalysis.

During the course of this work, a variety of alternative kinetic models were evaluated. These included specifically defined enzyme isomerization steps, consideration of cooperative binding and catalysis, and changes in the order of reversible and irreversible kinetic steps during both the burst and multiple-turnover phases of catalysis. Constraints introduced by requiring that the effective rate constant analysis (eq 3) must reproduce the experimentally determined V_{max} eliminated several of the alternative models from further consideration. In other cases, the alternative models failed to reproduce one or more key aspects of the experimental setup and results and were thus eliminated from further consideration. For example, rearrangement of the kinetic model of Figure 6 to place the first product release equilibrium after two successive, irreversible product formation steps led to an overestimation of the burst amplitude by ~2-fold and also failed to duplicate the experimental V_{max} when extrapolated into the steady-state time domain.

The coupling between reduced Fd and 18:1-ACP formation (Figure 3) can be understood by consideration of Figure 6. In these experiments, the oxidized enzyme−substrate complex (**2**) was mixed with reduced Fd to initiate catalysis by an electron-transfer step (k_{19}) within the catalytic loop that also includes a partially rate-limiting product release step (k_{15}). Thus, the effective rate of the combined single-turnover cycle was approximately equal to the autoxidation rate of reduced Fd leading to a progressive time-dependent decrease in reduced Fd concentration at the expense of further 18:1-ACP formation.

Studies with d_4-18:0-ACP. Most kinetic isotope effect studies of fatty acid desaturation have focused on the integral membrane superfamily of desaturases. From this previous work, primary kinetic isotope effects in the range of ~6−22 have been identified (*46*−*51*), which are considered to be suitable evidence for an overall rate limitation of the catalytic reaction by C−H(D) bond cleavage (*52*). Because the integral membrane enzymes and Δ9D share the same catalytic requirements for iron, O_2, and electron transfer and because each provides an overall identical outcome to catalysis, a detailed evaluation of the correspondence between these reaction mechanisms has been an important research goal in our laboratory.

Figure 6 predicts that V_{max} for Δ9D will be determined by the effective rate constant expression of eq 3. The forward commitment factor for V_{max} [$C_{vf} = k_{13}/(k_{18} + k_{19}) \approx 25$, with k_{18} negligible] indicates a relative insensitivity to deuterium substitution in 18:0-ACP. Correspondingly, previous kinetic isotope effect studies of Δ9D using either 9,9-d_2-7-thia-18:0-ACP or 10,10-d_2-7-thia-18:0-ACP found no significant primary $^{D}V_{max}$ effect during steady-state 18:1-ACP formation (*53*). This result is consistent with the presently identified dominating contributions of forward commitment, electron transfer, and product release to the effective rate of steady-state catalysis.

Nature of the Burst Phase. In the kinetic model of Figure 6, k_7 and k_{13} are assigned to irreversible steps of the Δ9D reaction. Due to experimental design, electron transfer and substrate binding are unlikely to correspond to the reaction step observed during the burst phase of catalysis. For reactions of prereduced Δ9D, comparison of the results obtained with 18:0-ACP and d_4-18:0-ACP revealed small decreases in the burst rate with the d_4-substrate. This result

indicates a primary kinetic isotope effect of $(k_H/k_D)(A_H/A_D) \approx 1.5$ on the burst phase of the reaction, k_7. Similarly, a modest $k_H/k_D \approx 1.4$ was observed in subsequent turnover of the second subunit of the Δ9D dimer, k_{13}. Thus, C−H bond cleavage is unlikely to contribute a significant rate limitation on either the burst reaction or the overall Δ9D reaction. However, by assuming the C_{vf} value indicated above, eq 4 (*54*)

$$^{D}V_{max} = 1.4 = (\text{intrinsic isotope effect} + C_{vf})/(1 + C_{vf}) \quad (4)$$

suggests an intrinsic isotope effect of ∼10 for the isotope-sensitive step, k_{13}. This calculated intrinsic value corresponds well with values anticipated a priori for a mechanism involving C−H(D) breakage. Other reaction steps that may contribute to the observed burst catalysis rate include enzyme conformational changes and reactions with O_2, with an interesting, albeit not substantiated, correlation between $k_{burst} \approx 95\ s^{-1}$ and the rate for reaction of $4e^-$ Δ9D and O_2 to give peroxo Δ9D, $k_{obsd} \approx 87\ s^{-1}$ (*13*).

Comparison with Other Soluble Diiron Enzymes. Table 2 compares reaction results for diiron enzymes. Primary deuterium isotope effects have been reported for the steady-state reaction of methane monooxygenase ($k_H/k_D \approx 1.7$) (*55*, *56*) and the rapid reaction of methane monooxygenase compound Q ($k_H/k_D \approx 80$) (*55*) with d_4-methane. Reactions with d_6-ethane and d_8-propane did not exhibit comparable isotope effects in the rapid reaction, presumably due to a decrease in the rate of substrate binding and a decrease in the activation barrier for C−H bond cleavage (104 kcal/mol for CH_3−H versus 95 kcal/mol for C_3H_7−H) (*57*, *58*). Hydrogen abstraction from 18:0-ACP by Δ9D was similarly masked by reaction steps other than C−H bond cleavage. The absence of a kinetic isotope effect in the reaction of the prereduced enzyme−substrate complex with O_2 and the apparent requirement of 18:0-ACP binding prior to O_2 activation indicate that steps leading to C−H bond activation limit k_{burst}.

A consideration of the physiological substrates and reactions of R2, methane monooxygenase, and Δ9D emphasizes important differences between these evolutionarily related enzymes. Prior to oxidation, each enzyme must correctly align the substrate for catalysis. In the case of R2, the substrate is a tyrosine residue positioned ∼5−8 Å from the diiron center (*59*) so that minimal positional adjustments are required for oxidation. Methane, an achiral substrate, can present four equivalent H atoms to compound Q, thus eliminating the requirement for stereospecific binding of the substrate in the active site. However, due to the thermodyamic stability of primary C−H bonds, optimal orbital alignment during the transition state is likely a key aspect of catalysis (*60*). For desaturation, Δ9D gives position-specific insertion of a cis double bond into the 18-carbon acyl chain. In part, the shape of the substrate channel (*15*) must facilitate formation of the cis isomer and contribute to the regiospecificity. In addition, Δ9D exhibits high stereospecificity for removal of the *9R* and *10R* hydrogen atoms (*22*), implying correct stereochemical positioning of the substrate relative to the diiron center. Ultimately, the coordination of protein conformational changes and diiron ligand rearrangements (*12*) with electron transfer and O_2 activation may lead to the catalytically relevant near-attack configuration (*61*). The present results suggest that several of these steps may provide rate-limiting contributions to the reaction mechanism.

REFERENCES

1. Shanklin, J., and Cahoon, E. B. (1998) *Annu. Rev. Plant Physiol. Plant Mol. Biol. 49*, 611−641.
2. Schultz, D. J., Cahoon, E. B., Shanklin, J., Craig, R., Cox-Foster, D. L., Mumma, R. O., and Medford, J. I. (1996) *Proc. Natl. Acad. Sci. U.S.A. 93*, 8771−8775.
3. Cahoon, E. B., Crammer, A. M., Shanklin, J., and Ohlrogge, J. B. (1994) *J. Biol. Chem. 269*, 27519−27526.
4. Cahoon, E. B., Shanklin, J., and Ohlrogge, J. B. (1992) *Proc. Natl. Acad. Sci. U.S.A. 89*, 11184−11188.
5. Fox, B. G., Shanklin, J., Somerville, C., and Munck, E. (1993) *Proc. Natl. Acad. Sci. U.S.A. 90*, 2486−2490.
6. Nordlund, P., and Ecklund, H. (1995) *Curr. Opin. Struct. Biol. 5*, 758−766.
7. Fox, B. G., Shanklin, J., Ai, J., Loehr, T. M., and Sanders-Loehr, J. (1994) *Biochemistry 43*, 12776−12786.
8. Wallar, B. J., and Lipscomb, J. D. (1996) *Chem. Rev. 96*, 2625−2657.
9. Fox, B. G. (1997) in *Comprehensive Biological Catalysis* (Sinnott, M., Ed.) pp 261−348, Academic Press, London, U.K.
10. Merkx, M., Kopp, D. A., Sazinsky, M. H., Blazyk, J. L., Muller, J., and Lippard, S. J. (2001) *Angew. Chem., Int. Ed. 40*, 2782−2807.
11. Lyle, K. L., Ai, J., Möenne-Loccoz, P., Sanders-Loehr, J., Loehr, T. M., and Fox, B. G. (2000) *Biochemistry 39*, 10507−10513.
12. Yang, Y., Broadwater, J. A., Pulver, S. C., Fox, B. G., and Solomon, E. I. (1999) *J. Am. Chem. Soc. 121*, 2770−2783.
13. Broadwater, J. A., Achim, C., Münck, E., and Fox, B. G. (1999) *Biochemistry 38*, 12197−12204.
14. Broadwater, J. A., Ai, J., Loehr, T. M., Sanders-Loehr, J., and Fox, B. G. (1998) *Biochemistry 37*, 14664−14671.
15. Lindqvist, Y., Huang, W., Schneider, G., and Shanklin, J. (1996) *EMBO J. 15*, 4081−4092.
16. Lee, S.-K., Nesheim, J. C., and Lipscomb, J. D. (1993) *J. Biol. Chem. 268*, 21569−21577.
17. Liu, K. E., Wang, D., Huynh, B. H., Edmondson, D. E., Salifoglou, A., and Lippard, S. J. (1994) *J. Am. Chem. Soc. 116*, 7465−7466.
18. Möenne-Loccoz, P., Baldwin, J., Ley, B. A., Loehr, T. M., and Bollinger, J. M., Jr. (1998) *Biochemistry 37*, 14659−14663.
19. Möenne-Loccoz, P., Krebs, K., Herlihy, K., Edmondson, D. E., Theil, E. C., Huynh, B. H., and Loehr, T. M. (1999) *Biochemistry 38*, 5290−5295.
20. Ling, J., Sahlin, M., Sjöberg, B.-M., Loehr, T. M., and Sanders-Loehr, J. (1994) *J. Biol. Chem. 269*, 5596−5601.
21. White, R. D., and Fox, B. G. (2001) *J. Inorg. Biochem. 86*, 479.
22. Behrouzian, B., Savile, C. K., Dawson, B., Buist, P. H., and Shanklin, J. (2002) *J. Am. Chem. Soc. 124*, 3277−3283.
23. Atkin, C. L., Thelander, L., Reichard, P., and Lang, G. (1973) *J. Biol. Chem. 248*, 7464−7472.
24. Sjöberg, B.-M., Reichard, P., Gräslund, A., and Ehrenberg, A. (1977) *J. Biol. Chem. 252*, 536−541.
25. Haas, J. A., and Fox, B. G. (1999) *Biochemistry 38*, 12833−12840.
26. Haas, J. A., and Fox, B. G. (2002) *Biochemistry 41*, 14472−14481.
27. Hoffman, B. J., Broadwater, J. A., Johnson, P., Harper, J., Fox, B. G., and Kenealy, W. R. (1995) *Protein Expression Purif. 6*, 646−654.
28. Cheng, H., Westler, W. M., Xia, B., Oh, B., and Markley, J. L. (1995) *Arch. Biochem. Biophys. 316*, 619−634.
29. Broadwater, J. A., and Fox, B. G. (1998) *Protein Expression Purif. 15*, 314−326.
30. Hill, R. B., MacKenzie, K. R., Flanagan, J. M., Cronan, J. E., and Prestegard, J. H. (1995) *Protein Expression Purif. 6*, 394−400.
31. Osborn, J. A., Jardine, F. H., Young, J. F., and G., W. (1966) *J. Chem. Soc.* 1711.
32. Fersht, A. (1985) *Enzyme Structure and Mechanism*, 2nd ed., W. H. Freeman, New York.
33. Duggleby, R. G. (1994) *Biochim. Biophys. Acta 1205*, 268−274.
34. Orme-Johnson, W. H., and Beinert, H. (1969) *Biochem. Biophys. Res. Commun. 36*, 905−911.
35. Cahoon, E. B., Lindqvist, Y., Schneider, G., and Shanklin, J. (1997) *Proc. Natl. Acad. Sci. U.S.A. 94*, 4872−4877.
36. Cleland, W. W. (1989) *Z. Naturforsch. 44A*, 445−449.

37. Cleland, W. W. (1975) *Biochemistry 14*, 3220−3224.
38. McKeon, T. A., and Stumpf, P. K. (1982) *J. Biol. Chem. 257*, 12141−12147.
39. Gibson, K. J. (1993) *Biochim. Biophys. Acta 1169*, 231−235.
40. Fox, B. G., Froland, W. A., Dege, J. E., and Lipscomb, J. D. (1989) *J. Biol. Chem. 264*, 10023−10033.
41. Froland, W. A., Andersson, K. K., Lee, S.-K., Liu, K., and Lipscomb, J. D. (1992) *J. Biol. Chem. 267*, 17588−17597.
42. Valentine, A. M., Stahl, S. S., and Lippard, S. J. (1999) *J. Am. Chem. Soc. 121*, 3867−3887.
43. Baldwin, J., Krebs, K., Ley, B. A., Edmondson, D. E., Huynh, B. H., and Bollinger, J. M. (2000) *J. Am. Chem. Soc. 122*, 12195−12206.
44. Schmidt, P. P., Rova, U., Katterle, B., Thelander, L., and Gräslund, A. (1998) *J. Biol. Chem. 273*, 21463−21472.
45. Lynch, J. B., Juarez-Garcia, C., Münck, E., and Que, L. J. (1989) *J. Biol. Chem. 264*, 8091−8096.
46. Schroepfer, G. J. J., and Bloch, K. (1965) *J. Biol. Chem. 240*, 54−63.
47. Morris, L. J. (1970) *Biochem. J. 118*, 681−693.
48. Enoch, H. G., Catala, A., and Strittmatter, P. (1976) *J. Biol. Chem. 251*, 5095−5103.
49. Buist, P. H., and Behrouzian, B. (1996) *J. Am. Chem. Soc. 118*, 6295−6296.
50. Buist, P. H., and Behrouzian, B. (1998) *J. Am. Chem. Soc. 120*, 871−876.
51. Abad, J. L., Camps, F., and Fabrias, G. (2000) *Angew. Chem., Int. Ed. 39*, 3279−3281.
52. Northrop, D. B. (1975) *Biochemistry 14*, 2644−2651.
53. Behrouzian, B., Buist, P. H., and Shanklin, J. (2001) *Chem. Commun. 5*, 401−402.
54. Northrop, D. B. (1981) *Annu. Rev. Biochem. 50*, 103−131.
55. Nesheim, J. C., and Lipscomb, J. D. (1996) *Biochemistry 35*, 10240−10247.
56. Rataj, M. J., Kauth, J. E., and Donnelly, M. I. (1991) *J. Biol. Chem. 266*, 18684−18690.
57. Brazeau, B. J., Wallar, B. J., and Lipscomb, J. D. (2001) *J. Am. Chem. Soc. 123*, 10421−10422.
58. Ambundo, E. A., Friesner, R. A., and Lippard, S. J. (2002) *J. Am. Chem. Soc. 124*, 8770−8771.
59. Nordlund, P., and Eklund, H. (1993) *J. Mol. Biol. 232*, 123−164.
60. Guallar, V., Gherman, B. F., Miller, W. H., Lippard, S. J., and Friesner, R. A. (2002) *J. Am. Chem. Soc. 124*, 3377−3384.
61. Bruice, T. C., and Benkovic, S. J. (2000) *Biochemistry 39*, 6267−6274.
62. Bollinger, J. M., Jr., Edmondson, D. E., Huynh, B. H., Filley, J., Norton, J. R., and Stubbe, J. (1991) *Science 253*, 292−298.
63. Yun, D., Krebs, K., Gupta, G., Iwig, D. F., Huynh, B. H., and Bollinger, J. M. (2002) *Biochemistry 41*, 981−990.
64. Bollinger, J. M., Tong, W. H., Ravi, N., Huynh, B. H., Edmondson, D. E., and Stubbe, J. (1994) *J. Am. Chem. Soc. 116*, 8015−8023.
65. Liu, Y., Nesheim, J. C., Lee, S.-K., and Lipscomb, J. D. (1995) *J. Biol. Chem. 270*, 24662−24665.
66. Shanklin, J., Whittle, E., and Fox, B. G. (1994) *Biochemistry 43*, 12787−12794.

BI030020O